Carrier-wave steepened pulses and gradient-gated high-order harmonic generation

S. B. P. Radnor, L. E. Chipperfield,* P. Kinsler,† and G. H. C. New
Blackett Laboratory, Imperial College London, Prince Consort Road, London SW7 2AZ, United Kingdom
(Received 15 May 2007; published 4 March 2008)

We show how to optimize the process of high-order harmonic generation (HHG) by gating the interaction using the field gradient of the driving pulse. Since maximized field gradients are efficiently generated by self-steepening processes, we first present a generalized theory of optical carrier-wave self-steepened (CSS) pulses. This goes beyond existing treatments, which only consider third-order nonlinearity, and has the advantage of describing pulses whose wave forms have a range of symmetry properties. Although a fertile field for theoretical work, CSS pulses are difficult to realize experimentally because of the deleterious effect of dispersion. We therefore consider synthesizing CSS-like profiles using a suitably phased subset of the harmonics present in a true CSS wave form. Using standard theoretical models of HHG, we show that the presence of gradient-maximized regions on the wave forms can raise the spectral cutoff and so yield shorter attosecond pulses. We study how the quality of the attosecond bursts created by spectral filtering depends on the number of harmonics included in the driving pulse.

DOI: 10.1103/PhysRevA.77.033806 PACS number(s): 42.65.Ky, 42.50.Hz, 32.80.Rm

I. INTRODUCTION

In high-order harmonic generation (HHG), the intensity maxima of a strong driving laser pulse tunnel-ionize an atom or molecule. Once an electron is in the continuum, its acceleration is controlled by the electric field profile $E(t)$. The electron is initially driven outward, but then the field reverses, driving it back for a high-energy recollision with the core, approximately three-quarters of a cycle later [1,2], in which an attosecond burst of extreme ultraviolet (xuv) radiation is generated. Indeed, each half-cycle of the driving pulse initiates this sequence of events, so a train of xuv bursts a few hundred attoseconds long is produced. While a train is useful for probing ultrafast dynamics, a primary goal of attosecond science is the generation of single bursts of xuv radiation and various gating schemes have been employed to achieve this. One scheme already in use is polarization gating [3–6]; in this technique, the sense of circular polarization reverses smoothly through the driving pulse, passing only briefly through linear polarization, at which point an attosecond burst is generated.

Another technique is to "gradient-gate" the HHG interaction, which can be done most simply by an additional driving field at double the frequency, suitably phased with respect to the fundamental field; this is just the case of two-color pumping [7–10]. In the present paper, we push the concept of gradient gating to its limits by considering how to achieve the steepest gradients possible. In principle, this can be done with carrier-wave steepening and shocking, a process first identified by Rosen [11] in 1965. He showed that for an instantaneous third-order ($\chi^{(3)}$) nonlinearity, field gradients could become infinite (i.e., shocks could form) after a finite distance of propagation. As we demonstrate in Sec. II, the theory can be extended to include arbitrary combinations of nonlinear terms, which opens up possibilities for controlling the symmetry of the pulse at the same time as generating a gradient gate. We then proceed to discuss the previously unaddressed second-order $\chi^{(2)}$ case, which turns out to give wave forms particularly useful for HHG.

Unfortunately it is very difficult to generate carrier-wave self-steepened (CSS) pulses because dispersion overwhelms the steepening process [12]. In Sec. III, we therefore discuss the possibility of synthesizing the steepened profiles by combining a suitably phased subset of the harmonics present in a true CSS profile; optical wave form synthesis of this kind is already exploited in other contexts (see, e.g., [13]). Such a synthesis is in any case a logical extension of both the two-color pumping scheme and the gradient-gate concept.

In Sec. IV, we compare simulations of HHG driven by standard pulses and by synthesized CSS-like wave forms. In the latter case, we demonstrate the importance of the relative phasing of the spectral components by comparing the results to those based on phase-flattened (i.e., field-maximized) pulses with equivalent spectral content. We also show that the efficacy of the synthesized profiles for HHG is progressively enhanced as the number of harmonics is increased. High-pass filtering then leads to the production of attosecond xuv bursts, and the presence of even harmonics in $\chi^{(2)}$ CSS-like pulses is shown to increase the degree of isolation of the bursts. A genetic algorithm is used to show that sawtooth profiles are ideal for driving HHG, which is in line with the general conclusions of this study, as summarized in Sec. V.

II. CARRIER-WAVE SELF-STEEPENING

The self-steepening of an optical pulse envelope was first studied by DeMartini *et al.* in 1967 [14] and is a well-known phenomenon associated with self-phase modulation. Surprisingly, however, the possibility of shock formation on the optical carrier was considered even earlier in a 1965 paper by Rosen [11], who showed that, for a third-order ($\chi^{(3)}$) nonlinearity, a field discontinuity (or shock) can develop under certain circumstances after a finite distance of propagation. Before a carrier shock forms or before its onset is halted by

*luke.chipperfield@imperial.ac.uk
†dr.paul.kinsler@physics.org

(e.g.) dispersion or the nonlinear response time, the carrier wave undergoes self-steepening. This phenomenon received little attention from the optics community for more than 30 years until it was reexamined in the 1990s by Flesch *et al.* [15,16], who performed finite-difference time-domain (FDTD) simulations of the process; more recently, the role of dispersion was examined in more detail [12].

The theory of carrier shocking and self-steepening is an important way of determining the profiles of pulses with a maximized field gradient and so is needed when considering the limits of a gradient-gated HHG scheme. Although a fertile field for theoretical work, CSS pulses are difficult to realize experimentally because of the deleterious effect of dispersion. Nevertheless, the theory provides important information when maximizing the gradient-gating effect in HHG.

A. General case

We use the method of characteristics (MOC) [17] to predict the shocking distance for a pulse in a dispersionless medium containing an arbitrary combination of nonlinear terms. The theory is based on the one-dimensional (1D), sourceless, plane-polarized Maxwell's equations for a field propagating in the z direction and a material response characterized by the electrical displacement field

$$D = \epsilon_0\left(E + \chi^{(1)}E + \sum_{m>1}\chi^{(m)}E^m\right), \tag{1}$$

where $\chi^{(m)}$ refers to the mth-order nonlinear susceptibility of the medium, which is assumed to be instantaneous. This extends the model used by Kinsler [18], since it allows for combinations of all orders of nonlinearity. Propagating pulses with a field profile $E(t)$ using this model lead to self-steepening of the carrier wave. Eventually, a localized *infinite* field gradient occurs on the wave form at a distance

$$S = -\min\left[\frac{2c\sqrt{n_0^2 + \sum_{q>1} q\chi^{(q)}E^{q-1}}}{\sum_{m>1} m\chi^{(m)}\frac{dE^{m-1}}{dt}}\right]. \tag{2}$$

Some exotic features of this prediction are discussed in [18].

To verify the predictions of Eq. (2), we used the pseudospectral spatial domain (PSSD) method [19] to propagate pulses for various orders of nonlinearity. The numerical shocks were detected using the local discontinuity detection (LDD) method [12], which is useful for shock detection within a discretized system. We also used a hybrid propagation technique, combining directional variables [20] and a wideband envelope [21], to check the results of the steepened and shocked wave forms. In all cases, the LDD (numerical) shocking distances obtained from our simulations were in good agreement with those predicted by Eq. (2).

Figure 1 illustrates typical CSS pulses for low-order nonlinearities and displays some striking properties. In particular, Figs. 1(a) and 1(c) (for $\chi^{(2)}$ and $\chi^{(4)}$) both have an underlying sawtooth shape, where the unit of repetition is a whole cycle. This is because both even *and* odd harmonics

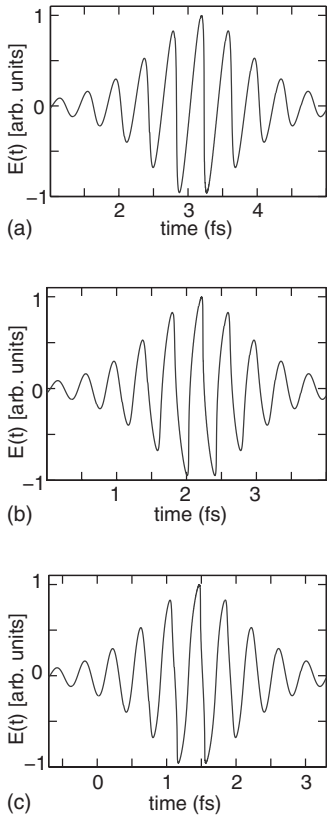

FIG. 1. Self-steepening at the LDD shocking distance for (a) $\chi^{(2)}$, (b) $\chi^{(3)}$, and (c) $\chi^{(4)}$ nonlinearities. Although a material with only a $\chi^{(4)}$ nonlinearity is not realistic, its inclusion helps illustrate some important features. We can test inversion symmetry by replacing E with $-E$. The initial pulse has $E=E_0\sin(\omega t+\phi_1)\mathrm{sech}(0.28\omega t/\tau)$, with a wavelength of 800 nm, $\phi_1=0$, and $\tau=1$; $n_0=1$. The nonlinear strength is $\chi^{(n)}E^{n-1}=0.02$.

are present in the spectrum and the inversion symmetry of the initial pulse is broken; positive lobes of $E(t)$ lean to later times and negative lobes to earlier times, since (for $\chi^{(2)}$) the change in characteristic velocity is proportional to dE/dt and (for $\chi^{(4)}$) to dE^3/dt. In contrast, Fig. 1(b) (for $\chi^{(3)}$) shows both positive and negative lobes leaning to later times, since the change in characteristic velocity is proportional to dE^2/dt. Because odd nonlinearities produce a cascade containing *only* odd harmonics, every half-cycle is similar and the pulses preserve inversion symmetry. Another noteworthy feature is that, for higher-order nonlinearities, the steepening becomes increasingly localized to within the most intense carrier oscillation(s).

B. Special case: $\chi^{(2)}$ CSS pulses

We now present a brief review of self-steepening and shocking for $\chi^{(2)}$ nonlinearities. We focus on this case because it has not previously been addressed and because of the relevance to HHG discussed later in Sec. IV. Of course, nonlinearities of higher order than third also exist (see, e.g., [22]), but usually they are much less important. The $\chi^{(3)}$ case has already been extensively addressed in the literature [11,12,15,16]. For a $\chi^{(2)}$ nonlinearity on its own, Eq. (2)

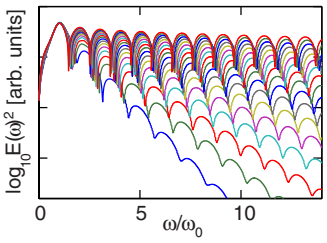

FIG. 2. (Color online) Logarithmic plot of $E(\omega)^2$ every half micron, approaching S_2 in a $\chi^{(2)}$ material. The spectra flatten out as increasing amounts of ever higher-order harmonics are generated as the pulse approaches the shock. The pulse and material parameters are as for Fig. 1. Each ordinate division represents five orders of magnitude.

indicates that the shocking distance depends primarily on the inverse field gradient so that $S_2 \propto \min|dE/dt|^{-1}$.

A profile for a (nearly shocked) $\chi^{(2)}$ CSS pulse in a dispersionless medium can be seen in Fig. 1(a), with its characteristic sawtooth profile. It exhibits two distinct regions: one containing a ramplike smooth progression from negative to positive field values taking up the majority of the cycle and the second with a rapid positive to negative transition over the remaining small fraction of the cycle. If we plotted the wave form for a continuous wave field, rather than a pulse, we would see the field evolving toward a sawtoothlike profile (e.g., as seen in [18]).

The buildup of harmonic content during the reshaping and steepening of the time domain profiles is vividly illustrated in Fig. 2. Note that the spectra differ from those produced under $\chi^{(3)}$ self-steepening where only odd harmonics are produced. The nature of the harmonic cascade in Fig. 2 indicates that, if it were possible to achieve strong self-steepening experimentally, this would in itself be a route to HHG. We will return to this point in the next section.

As for the $\chi^{(3)}$ case [12], the $\chi^{(2)}$ process is also sensitive to the pulse length and the carrier envelope phase (CEP) offset; these parameters are also important when driving HHG. Figure 1(a) shows that for a CEP of $\phi_1=0$, the carrier has a positive gradient at the center of the pulse. However, steepening occurs for negative gradients in the $\chi^{(2)}$ case, and hence the high gradients occur near the zeros half a cycle away on either side. Since these are reduced by envelope falloff, S_2 increases as the pulse width is reduced for $\phi_1=0$. In contrast, when $\phi_1=\pi$, steepening occurs at the center of the pulse and S_2 is then independent of pulse duration. The dependence of S_2 on CEP for different pulse widths is shown in Fig. 3. This can be compared with the more complicated CEP dependence seen in Fig. 4 of [12], where $S_3 \propto \min|dE^2/dt|^{-1}$.

III. GENERATING CSS PULSES

The theory of Sec. II was based on the ideal case of a dispersionless medium with instantaneous nonlinearity. The question of whether sufficiently self-steepened pulses could be generated in *real* nonlinear materials has been addressed for the $\chi^{(3)}$ case in [15,16], where considerations such as

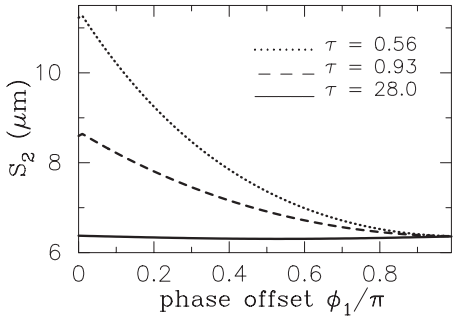

FIG. 3. MOC shocking distances S_2 as a function of CEP ϕ, allowing for different pulse widths. In the long pulse ($\tau=28$) case, a shallow minimum centered around $\phi_1=\pi/2$ is just visible, caused by the term in the square root of Eq. (2). Apart from the varying pulse length, the pulse and material parameters are as for Fig. 1.

linear dispersion [12] and the strength and response time of the nonlinearities were evaluated. Similar issues arise in the $\chi^{(2)}$ case, and so we will not repeat them here. We note that for many $\chi^{(2)}$ materials, the polarization of the generated harmonics is different from that of the driving field, bringing in the further complication of birefringence. However, materials do exist that support processes where the polarizations are the same (e.g., $e+e \rightarrow e$ in lithium niobate [23]), which could (in principle) generate a harmonic cascade in a single polarization.

In practice, the limitations imposed by dispersion and material damage mean that generating strongly self-steepened pulses would be an extremely challenging task, although some success might be achieved if relatively weak self-steepening were sufficient. We therefore consider the possibility of *synthesizing* CSS-like pulses by combining a subset of harmonic components using the phase offsets and amplitudes obtained from numerically generated CSS profiles. It turns out to be possible to approximate $\chi^{(2)}$ and $\chi^{(3)}$ CSS-like wave forms using field strengths and phases for the nth harmonic ($n>1$) based on the formulas

$$E_n = F^{-\sqrt{n-1}} E_1, \tag{3}$$

$$\phi_n = n\phi_1 + (n-1)\pi/N, \tag{4}$$

where $n(>1)$ is the harmonic order, $N=2$ or 3 for the $\chi^{(2)}$ and $\chi^{(3)}$ cases, respectively, and F is a fitting factor. With $F=4$, these equations give a reasonable match to the CSS wave form with the spectrum fourth from the top in Fig. 2, which is close to shocking. We note that higher-order harmonics comprise only a small fraction of the total CSS pulse energy. However, only a small number of harmonics would be used in a synthesized pulse. Quite apart from the experimental complexity involved in combining a large number of harmonics, the HHG experiment would be pointless if the high harmonics were available already in the driving pulse. As we will show in Sec. IV, sufficient gradient enhancement can be achieved with a driving pulse containing only two or three additional harmonic components.

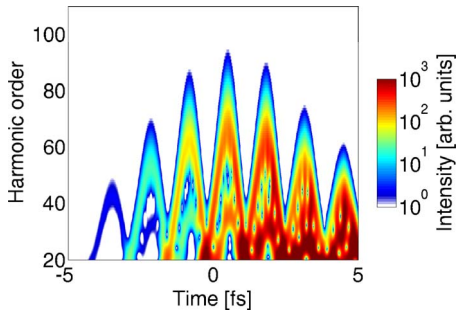

FIG. 4. (Color online) Wavelet transform of the HHG from a normal driving pulse with $\lambda=800$ nm, an 8-fs FWHM with peak intensity 5×10^{14} W/cm^2. Since the driving pulse retains inversion symmetry, high harmonics with a similar distribution are generated every half-cycle. Note that the center of the pulse produces the bulk of the HHG, which [following Eq. (5)] depends on E^2. The 1D TDSE model of HHG was used to generate this figure.

IV. HHG AND CSS PULSES

As described in the Introduction, the bursts of xuv radiation produced in the electron ionization-recollision process that occurs when an intense few-cycle laser pulse interacts with an atom contain a wide range of high-order harmonics. HHG experiments aiming to produce isolated attosecond bursts are typically based on few-cycle driving pulses, but a number of sophisticated techniques have also been deployed, including the use of two-color driving fields [7–10], polarization gating [3–6], and chirp control [24].

A typical HHG spectrum from an atomic gas consists of a broad plateau of harmonics extending to high orders, which falls off rapidly above a cutoff energy $\mathcal{E}$. For monochromatic driving fields [1,2,25],

$$\mathcal{E} = I_P + 3.17U_P, \tag{5}$$

where I_P is the ionization potential of the atom, $U_P = E_1^2/(2m_e\omega)^2$ is the ponderomotive potential of the laser field, and E_1 is the maximum field strength. The atom used for all the simulations in this paper was neon, which has a U_P of 21.6 eV. Equation (5) suggests that $\mathcal{E}$ can be increased either by increasing E_1 or by using an atomic species with a higher I_P. However, raising E_1 also enhances the ionization rate, and this in turn can deplete the ground state, causing defocusing of the laser beam and a reduction in HHG.

For few-cycle driving pulses, the parameters naturally change from one half-cycle to the next. This feature is highlighted in Fig. 4, where a wavelet transform displays the variation of the harmonic spectrum for an 8-fs driving pulse, calculated using the 1D time-dependent Schrödinger equation (TDSE) model [26]. For pulsed (or multicolor) excitation, the strong field approximation (SFA) [27] predicts the spectral cutoff energy to be the maximum value of the function [28]

$$\mathcal{E}(t_i,t_r) = I_P + \frac{1}{2}[eA(t_r) + p(t_i,t_r)]^2, \tag{6}$$

where t_i is the ionization time, t_r is the recollision time, $A(t)$ is the vector potential, and p is the *asymptotic* momentum of the electron. Equation (6) reproduces Eq. (5) in the case of a monochromatic field. For electrons that both ionize and recombine at the position of the core,

$$p(t_i,t_r) = -\frac{e}{t_r - t_i}\int_{t_i}^{t_r} A(t)dt. \tag{7}$$

Although a general interpretation of Eq. (6) is complicated, the electron trajectories that are of most importance for HHG are those for which the initial momentum of the electron $[p(t_i,t_r)+eA(t_i)]$ is close to zero. In this case, $p(t_i,t_r)=-eA(t_i)$, so that Eq. (6) simplifies to $\mathcal{E}=I_P+[eA(t_r)-eA(t_i)]^2/2$. Usually $A(t_i)$ is small, so it is broadly true to say that $\mathcal{E}$ depends on the peak value of $A(t_r)$. And since the second time derivative of A and, concomitantly, the first time derivative of E tend to follow A, the implication is that maximizing the *gradient* of the field will raise the allowed peak value of $A(t_r)$. Since CSS-like pulses have strongly steepened field gradients, they should therefore produce HHG with a raised cutoff energy $\mathcal{E}$ and an increased number of harmonics.

A. HHG using synthesized driving pulses

To create a two-color driving field, a second harmonic component is added so that

$$E(t) = E_1\cos(\omega t + \phi_1) + E_2\cos(2\omega t + \phi_2), \tag{8}$$

where we will assume that $\phi_1=0$ for simplicity. The addition of the second harmonic term causes inversion symmetry of the profile to be lost. If $\phi_2=0$, the positive and negative lobes of the field have different peak amplitudes, leading to different levels of tunnel ionization on alternate half-cycles and associated variations in the intensity and cutoff of the HHG spectrum. On the other hand, when $\phi_2=\pi/2$, it is the positive and negative *slopes* of E that differ, along with the positive and negative excursions of A and d^2A/dt^2. Once again, the effect is to maximize $\mathcal{E}$ every other half-cycle [10], but the effect is now substantially stronger than in the $\phi_2=0$ case.

More complex fields can be synthesized by adding further harmonics, with each additional component providing a significant boost to the field gradient. However, as we shall see in Sec. IV C below, the benefits are eventually subject to the law of diminishing returns. Pulse profiles containing even as well as odd harmonics invariably exhibit characteristics that alternate from one half-cycle to the next. This feature is clearly evident in Fig. 5 where the wavelet transform of the HHG generated by a $\chi^{(2)}$ CSS-like pulse spectrally truncated above the sixth harmonic is displayed; details are given in the caption. The figure should be compared with Fig. 4. If a high-pass filter (such as a molybdenum-silicon multilayer mirror) is applied to the signal of Fig. 5, the lower peaks can be removed, leaving the highest peak(s) in greater isolation. As such, these filters are useful for the generation of a single xuv burst or when creating burst trains for stroboscopic imaging [29].

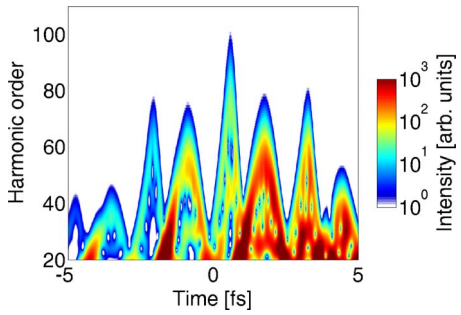

FIG. 5. (Color online) Wavelet transform of the HHG from a synthesized $\chi^{(2)}$ CSS-like driving pulse using amplitudes and phases from Eqs. (3) and (4) with $F=4$ and spectral contributions above the sixth harmonic removed. The energy and other relevant characteristics of the driving pulse are same as for Fig. 4. It clearly shows the alternating emission from each half cycle of the steepened pulse. The 1D TDSE model of the HHG process was used to generate this figure.

B. Phasing of the harmonic components

Increasing the number of harmonics naturally increases the experimental complexity, and arranging for their correct phasing makes the situation even more complicated. It is therefore important to check that CSS-like pulses are better for HHG because of their steep field gradients, rather than simply because of their greater harmonic content. Is the mere presence of many harmonics (irrespective of their phase) the crucial thing, or will a restricted range of harmonics, correctly phased to maximize the gradient, perhaps yield a better result with less experimental effort?

To address this issue, we compare HHG spectra for different types of driving pulse in Fig. 6. Reading from top to bottom, spectra are shown for (i) a synthesized CSS-like pulse containing third and fifth harmonics (labeled $\chi^{(3)}$ CSS); (ii) a synthesized CSS-like pulse containing second, third, and fourth harmonics (labeled $\chi^{(2)}$ CSS); (iii) a "field-maximized spectrum" (FMS) pulse containing identical spectral content to the $\chi^{(2)}$ CSS pulse, but with phases $\phi_n=0$, to create a maximized field rather than a maximized gradient; and (iv) a normal quasimonochromatic pulse similar to the one used to create Fig. 4.

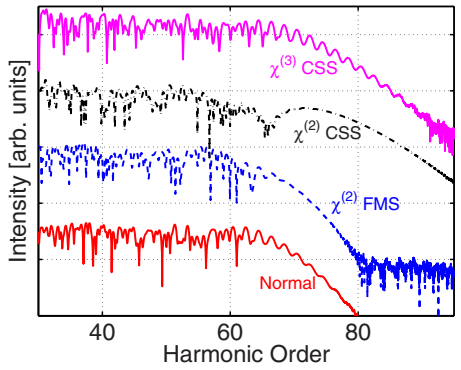

FIG. 6. (Color online) HHG spectra for different driving pulses, offset vertically for clarity. Each ordinate division represents four orders of magnitude. The pulse energy and other relevant characteristics are the same as for Fig. 4. The synthesized $\chi^{(2)}$ FMS and CSS pulses contain second, third, and fourth harmonics; the synthesized $\chi^{(3)}$ CSS pulse contains third and fifth harmonics. Bottom curve to top curve: normal (red), $\chi^{(2)}$ FMS (blue), $\chi^{(2)}$ CSS (black), and $\chi^{(3)}$ CSS (magenta).

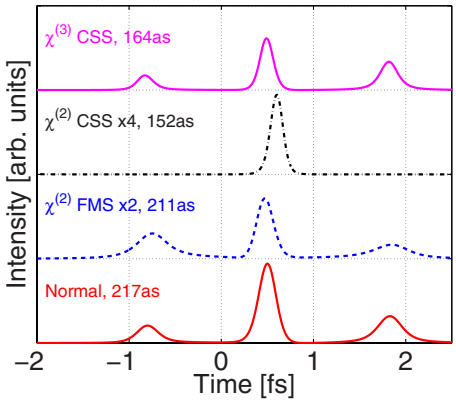

FIG. 7. (Color online) xuv burst intensity profiles and FWHM resulting from high-pass-filtered HHG spectra for the various CSS driving pulses seen in Fig. 6. Bottom curve to top curve: normal (red), $\chi^{(2)}$ FMS (blue), $\chi^{(2)}$ CSS (black), and $\chi^{(3)}$ CSS (magenta). The curves have been individually scaled to aid visibility.

The benefit of a gradient-maximized pulse over both the normal and FMS pulses is demonstrated vividly in the figure. The highest $\mathcal{E}$ is clearly obtained for the $\chi^{(2)}$ CSS pulse. Further, a comparison of $\chi^{(2)}$ CSS, $\chi^{(2)}$ FMS, and the normal spectra reveals that the CSS pulses have the most gradual cutoff. The conclusion is that optimum performance results from the character of the CSS profiles and not merely their harmonic content.

Figure 7 shows the temporal profiles of attosecond xuv bursts obtained by appropriate filtering of the four HHG spectra of Fig. 6. In each case, the filtering was adjusted to minimize the full width at *one-quarter* maximum, a procedure that created the cleanest pulses. It is clear that a $\chi^{(2)}$ CSS driving pulse produces the shortest and most isolated xuv bursts, although the intensity is lower than in the $\chi^{(2)}$ FMS case where there is one strong and one weak burst per cycle. The $\chi^{(3)}$ CSS pulse produces *two* short xuv bursts per cycle, with a relatively high intensity. We note that the oscillations in the tails of the $\chi^{(3)}$ CSS spectra in Fig. 6 are associated with the presence of more than one xuv burst, as seen in Fig. 7.

C. Optimum number of harmonics

As mentioned earlier, moving from standard single-color to two-color pumping adds experimental complexity and the situation will naturally be exacerbated if additional harmonics are included. It is therefore important to study how effectively the extra experimental investment is reflected in improved HHG performance.

Figures 8 and 9 demonstrate what happens when HHG is driven by $\chi^{(2)}$ and $\chi^{(3)}$ CSS-like pulses as the number of harmonic components is increased. In each case, there is

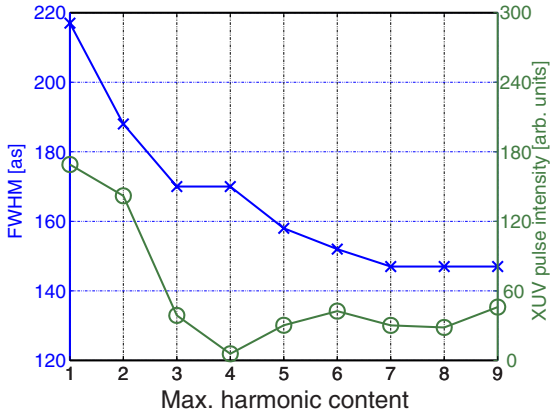

FIG. 8. (Color online) xuv burst durations and intensities resulting from high-pass-filtered HHG spectra for synthesized $\chi^{(2)}$ CSS-like driving pulses, as a function of the maximum harmonic component included. The burst durations are denoted with × and use the left-hand scale; the intensities are denoted with ○ and use the right-hand scale. The 1D TDSE model was used.

clearly a strong initial reduction in the burst durations as extra harmonics are added. The FWHM decreases roughly linearly up to about the fifth harmonic, but the graphs flatten out thereafter. The intensity of the bursts drops off rapidly too, although this is not necessarily a serious consideration; after all, much intensity is also lost in polarization-gating schemes. Different filtering strategies (e.g., allowing lower frequencies through) can provide shorter xuv bursts than shown in Fig. 8, but this usually results in stronger satellite pulses.

D. Optimum field profile

The fact that $\chi^{(2)}$ CSS pulses succeed in maximizing the HHG cutoff energy $\mathcal{E}$ at a given pulse energy is due to the way in which the particular electric field profile controls the

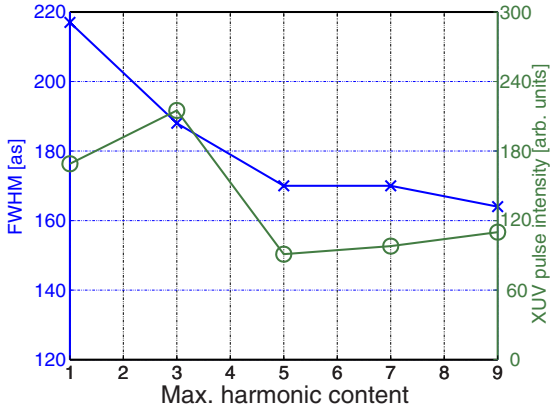

FIG. 9. (Color online) xuv burst durations and intensities resulting from high-pass-filtered HHG spectra for synthesized $\chi^{(3)}$ CSS-like driving pulses, as a function of the maximum harmonic component included. The burst durations are denoted with × and use the left-hand scale; the intensities are denoted with ○ and use the right-hand scale. The 1D TDSE model was used.

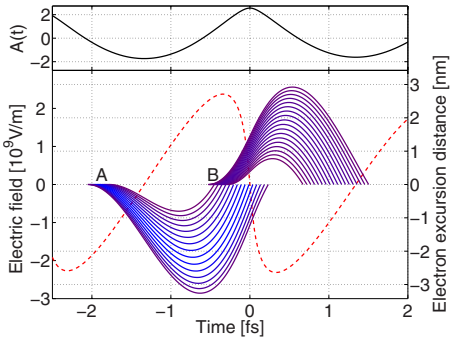

FIG. 10. (Color online) Upper frame: the vector potential $A(t)$ corresponding to the field profile shown in the lower frame. Note how the peaks in $A(t)$ correspond to the regions of high field gradient. Lower frame: the trajectories of *only* those high-energy ionized electrons that recollide with the nucleus to emit high-order harmonic radiation, calculated using the SFA model [27]. The dashed (red) line shows the CSS field profile, in this case for the center of a three-cycle pulse with peak intensity 5×10^{14} W/cm^2. The CSS-enhanced trajectories (starting at A, on the left) recollide over a short period of time at high field gradients, giving rise to a brief xuv emission with larger cutoff energy. The latter set of recolliding trajectories (starting at B, right) have a lower energy and recollide over a longer time interval at low field gradients.

motion of the ionized electrons. As shown in Fig. 10, the outward journey and initial deceleration of the electrons in group A are determined by the shallow ramp of the field as it rises gently from negative to positive. The high return acceleration is managed by the high-field region, and the subsequent steep field decrease allows the electrons to recollide with the core within minimal deceleration, while simultaneously resetting the field amplitude so that the process can repeat. The overall effect is to create trajectories that minimize the distance traveled, while ensuring the highest possible recollision energies along with a high $\mathcal{E}$. The high-energy recollisions take place largely during the brief high-gradient part of the field profile and give rise to the narrow peaks in Fig. 5, which then become the short duration xuv bursts of Fig. 7 after high-pass filtering.

A genetic algorithm [30] used in combination with classical simulations of electron trajectories has confirmed that the sawtoothlike $\chi^{(2)}$ CSS profiles are uniquely efficient for HHG. Using parametrized field profiles, we sought to optimize the recollision energy while holding both the pulse energy per cycle and the periodicity fixed. The algorithm consistently predicted that the optimum wave form was a linear ramp starting at a field $-E_{\max}/2$ and increasing to $E_{\max}$. This corresponds to the last three quarter-cycles of a sawtooth wave form; indeed, in Fig. 10 we can see that SFA predictions for the CSS-enhanced trajectories agree with the classical picture and start at about a quarter-cycle in. Adding a dc bias or sufficiently low-frequency field to a $\chi^{(2)}$ CSS-like profile might therefore make fuller use of the whole ramp section of the wave form, further increasing $\mathcal{E}$.

A second family of ionization-recollision trajectories (group B in Fig. 10) are initiated during the high field region of the optical cycle. However, these recollisions occur in a region of lower field, produce lower recollision energies, and

are spread over a longer time interval. They lead to more intense but longer HHG emission, with a low $\mathcal{E}$, represented by the broader and lower peaks in Fig. 5.

Returning to Figs. 8 and 9, we see that the change in burst duration (or intensity) for each additional harmonic component is not necessarily straightforward or monotonic. This serves to illustrate that the HHG dynamics is complicated and that the general principle of maximizing the field gradient could be optimized by further use of a genetic algorithm. Indeed, any HHG model could be optimized for a specific outcome—e.g., for the shortest-duration xuv burst. It would also allow the potential benefits of spectral inputs other than the harmonic cascade used here to be evaluated.

V. CONCLUSION

We have shown how to optimize HHG using gradient gating of the interaction and that CSS pulses (or in practice their synthesized counterparts) are the most efficient way of providing the localized steep field gradients needed. An important conclusion is that the gradient-gated HHG enhancement can be achieved using as few as three or four correctly phased extra harmonic components. The study was assisted by our generalized theory of optical carrier-wave self-steepening. By describing wave forms generated by a $\chi^{(2)}$ nonlinear interaction, the theory showed how their advantageous symmetry properties could be used to generate shorter, more isolated xuv bursts. By using a genetic algorithm with selection based on the recollision energy of classical electrons, we confirmed that indeed the sawtoothlike $\chi^{(2)}$ CSS pulses do have an optimal form that increased the HHG cutoff energy $\mathcal{E}$ for any given pulse energy.

In summary, we have shown that the use of CSS-like driving pulses for HHG has the potential to generate shorter, more isolated xuv bursts, as well as suggesting possibilities for other HHG optimization schemes.

ACKNOWLEDGMENT

The authors acknowledge financial support received from the Engineering and Physical Sciences Research Council (U.K.).

[1] K. J. Schafer, B. Yang, L. F. DiMauro, and K. C. Kulander, Phys. Rev. Lett. **70**, 1599 (1993).
[2] P. B. Corkum, Phys. Rev. Lett. **71**, 1994 (1993).
[3] K. S. Budil, P. Salières, A. L'Huillier, T. Ditmire, and M. D. Perry, Phys. Rev. A **48**, R3437 (1993).
[4] P. B. Corkum, N. H. Burnett, and M. Y. Ivanov, Opt. Lett. **19**, 1870 (1994).
[5] I. J. Sola, E. Mével, L. Elouga, E. Constant, V. Strelkov, L. Poletto, P. Villoresi, E. Benedetti, J.-P. Caumes, S. Stagira, C. Vozzi, G. Sansone, and M. Nisoli, Nat. Phys. **2**, 319 (2006).
[6] G. Sansone, E. Benedetti, F. Calegari, C. Vozzi, L. Avaldi, R. Flammini, L. Poletto, P. Villoresi, C. Altucci, R. Velotta, S. Stagira, S. De Silvestri, and M. Nisoli, Science **314**, 443 (2006).
[7] T. T. Liu, T. Kanai, T. Sekikawa, and S. Watanabe, Phys. Rev. A **73**, 063823 (2006).
[8] Y. Oishi, M. Kaku, A. Suda, F. Kannari, and K. Midorikawa, Opt. Express **14**, 7230 (2006).
[9] H. Merdji, T. Auguste, W. Boutu, J.-P. Caumes, B. Carré, T. Pfeifer, A. Jullien, D. M. Neumark, and S. R. Leone, Opt. Lett. **32**, 3134 (2007).
[10] T. Pfeifer, L. Gallmann, M. J. Abel, D. M. Neumark, and S. R. Leone, Opt. Lett. **31**, 975 (2006).
[11] G. Rosen, Phys. Rev. **139**, A539 (1965).
[12] P. Kinsler, S. B. P. Radnor, J. C. A. Tyrrell, and G. H. C. New, Phys. Rev. E **75**, 066603 (2007).
[13] Z. Jiang, C.-B. Huang, D. E. Leaird, and A. M. Weiner, Nat. Photonics **1**, 463 (2007).
[14] F. DeMartini, C. H. Townes, T. K. Gustafson, and P. L. Kelley, Phys. Rev. **164**, 312 (1967).
[15] R. G. Flesch, A. Pushkarev, and J. V. Moloney, Phys. Rev. Lett. **76**, 2488 (1996).
[16] L. Gilles, J. V. Moloney, and L. Vazquez, Phys. Rev. E **60**, 1051 (1999).
[17] G. B. Whitham, *Lectures on Wave Propagation* (Wiley, New York, 1979).
[18] P. Kinsler, J. Opt. Soc. Am. B **24**, 2363 (2007); detailed MOC calculations are given in the Appendixes of e-print arXiv:0707.0986.
[19] J. C. A. Tyrrell, P. Kinsler, and G. H. C. New, J. Mod. Opt. **52**, 973 (2005).
[20] P. Kinsler, S. B. P. Radnor, and G. H. C. New, Phys. Rev. A **72**, 063807 (2005).
[21] G. Genty, P. Kinsler, B. Kibler, and J. M. Dudley, Opt. Express **15**, 5382 (2007).
[22] Y.-F. Chen, K. Beckwitt, F. W. Wise, B. G. Aitken, J. S. Sanghera, and I. D. Aggarwal, J. Opt. Soc. Am. B **23**, 347 (2006).
[23] S. G. Grechin, V. G. Dmitriev, and Yu. V. Yur'ev, Quantum Electron. **29**, 155 (1999).
[24] R. A. Ganeev, M. Suzuki, P. V. Redkin, M. Baba, and H. Kuroda, Phys. Rev. A **76**, 023832 (2007).
[25] J. L. Krause, K. J. Schafer, and K. C. Kulander, Phys. Rev. Lett. **68**, 3535 (1992).
[26] L. E. Chipperfield, P. L. Knight, J. W. G. Tisch, and J. P. Marangos, Opt. Commun. **264**, 494 (2006).
[27] M. Lewenstein, Ph. Balcou, M. Yu. Ivanov, A. L'Huillier, and P. B. Corkum, Phys. Rev. A **49**, 2117 (1994).
[28] C. A. Haworth, L. E. Chipperfield, J. S. Robinson, P. L. Knight, J. P. Marangos, and J. W. G. Tisch, Nat. Phys. **3**, 52 (2007).
[29] T. Remetter, P. Johnsson, J. Mauritsson, K. Varjú, Y. Ni, F. Lépine, E. Gustafsson, M. Kling, J. Khan, R. López-Martens, K. J. Schafer, M. J. J. Vrakking, and A. L'Huillier, Nat. Phys. **2**, 323 (2006).
[30] S. Forrest, Science **261**, 872 (1993).